

**PL-TR-96-2035**

**INCOHERENT SCATTER VERIFICATION  
OF DMSP OBSERVATIONS**

Jeffrey P. Thayer

SRI International  
333 Ravenswood Avenue  
Menlo Park, CA 94025

December 1995

Scientific Report No. 1

Approved for public release; distribution unlimited

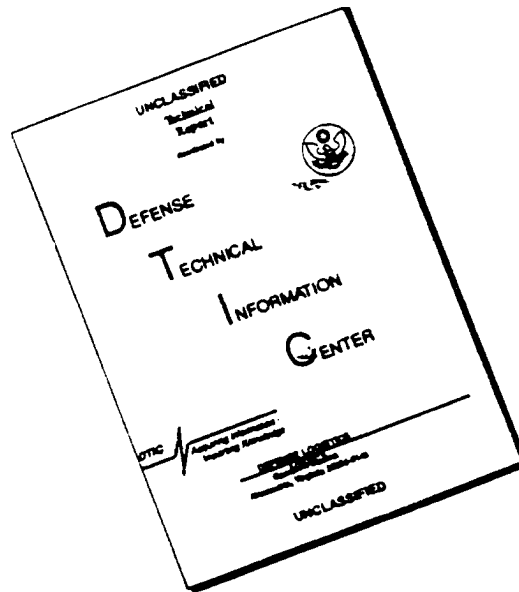
19960322 113



**PHILLIPS LABORATORY  
Directorate of Geophysics  
AIR FORCE MATERIEL COMMAND  
HANSCOM AFB, MA 01731-3010**

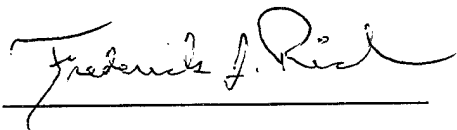
DECLASSIFIED AUTHORITY: [illegible]

# DISCLAIMER NOTICE



THIS DOCUMENT IS BEST QUALITY AVAILABLE. THE COPY FURNISHED TO DTIC CONTAINED A SIGNIFICANT NUMBER OF PAGES WHICH DO NOT REPRODUCE LEGIBLY.

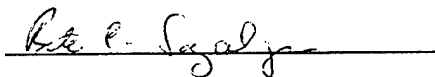
"This Technical report has been reviewed and is approved for publication"



FREDERICK RICH  
Contract Manager



EDWARD G. MULLEN  
Branch Chief



RITA C. SAGALYN  
Division Director

This report has been reviewed by the ESC Public Affairs Office (PA) and is releasable to the National Technical Information Service (NTIS).

Qualified requestors may obtain additional copies from the Defense Technical Information Center (DTIC). All others should apply to the National Technical Information Service (NTIS).

If your address has changed, or if you wish to be removed from the mailing list, or if the addressee is no longer employed by your organization, please notify PL/IM, 29 Randolph Road, Hanscom AFB, MA 01731-3010. This will assist us in maintaining a current mailing list.

Do not return copies of this report unless contractual obligations or notices on a specific document requires that it be returned.

REPORT DOCUMENTATION PAGE			Form Approved OMB No. 0704-0188	
Public reporting burden for this collection of information is estimated to average 1 hour per response, including the time for reviewing instructions, searching existing data sources, gathering and maintaining the data needed, and completing and reviewing the collection of information. Send comments regarding this burden estimate or any other aspect of this collection of information, including suggestions for reducing this burden, to Washington Headquarters Services, Directorate for Information Operations and Reports, 1215 Jefferson Davis Highway, Suite 1204, Arlington, VA 22202-4302, and to the Office of Management and Budget, Paperwork Reduction Project (0704-0188), Washington, DC 20503.				
1. AGENCY USE ONLY (Leave Blank)	2. REPORT DATE December 1995	3. REPORT TYPE AND DATES COVERED Scientific No. 1		
4. TITLE AND SUBTITLE Incoherent Scatter Verification of DMSP Observations			5. FUNDING NUMBERS PE 35160F PR 1924 TA GB WU MC Contract F19628-94-C-0100	
6. AUTHORS Jeffrey P. Thayer				
7. PERFORMING ORGANIZATION NAME(S) AND ADDRESS(ES) SRI International 333 Ravenswood Avenue Menlo Park, CA 94025-3493			8. PERFORMING ORGANIZATION REPORT NUMBER	
9. SPONSORING/MONITORING AGENCY NAME(S) AND ADDRESS(ES) Phillips Laboratory 29 Randolph Road Hanscom AFB, MA 01731-3010 Contract Manager: Frederick Rich/GPSP			10. SPONSORING/MONITORING AGENCY REPORT NUMBER PL-TR-96-2035	
11. SUPPLEMENTARY NOTES				
12a. DISTRIBUTION/AVAILABILITY STATEMENT Approved for public release; distribution unlimited			12b. DISTRIBUTION CODE	
13. ABSTRACT (Maximum 200 words) <p>The transfer of electromagnetic energy to heat, i.e., Joule heating, in the ionospheric gas is often the most dominant energy source for the polar regions. The Defense Meteorological Satellite Program (DMSP) has demonstrated that the Joule heating rate in the high-latitude ionosphere can be estimated with measurements of the perturbation magnetic field and precipitating particle population. These estimates of the Joule heating rate are subject to a number of assumptions and empirical formalisms that require validation. The NSF incoherent-scatter radar located at Sondrestrom, Greenland, can measure the plasma parameters of interest and is at a latitude well-suited for coincident measurements with DMSP. Recent radar improvements in altitude resolution and signal statistics in the E region has permitted the Joule heating rate to be more accurately determined than ever before. Also, the manner in which the Joule heating rate is now being calculated parallels that of DMSP allowing a more direct means of testing assumptions and comparing results. Here, we summarize the progress made over the program year and detail the observational program for conjunctions with the F12 and F13 DMSP satellites and the radar.</p>				
14. SUBJECT TERMS high-latitude ionosphere Joule heating rate			15. NUMBER OF PAGES 24	
			16. PRICE CODE	
17. SECURITY CLASSIFICATION OF REPORT Unclassified	18. SECURITY CLASSIFICATION OF THIS PAGE Unclassified	19. SECURITY CLASSIFICATION OF ABSTRACT Unclassified	20. LIMITATION OF ABSTRACT SAR	

## 1. Introduction

The high-latitude E region is subject to several sources of energy—that is, solar UV/EUV radiation, electromagnetic energy (resulting in Joule heating and mechanical energy transfer), particle precipitation, atmospheric waves and tides, and magnetospheric waves. At times and for specific altitudes within the E region, any of these energy sources, expressed in terms of energy flux ( $\text{Wm}^{-2}$ ), may dominate. Of these, the magnetospheric sources have the most profound effect on the high-latitude E region with, for example, the Joule heating rate and the heating rate due to particle precipitation (each reaching  $100 \text{ mWm}^{-2}$ ), far exceeding direct heating by solar EUV energy ( $1$  to  $3 \text{ mWm}^{-2}$ ) within the auroral oval [e.g., Banks, 1977]. Although Joule heating and particle heating are closely linked features of the high-latitude E region, their impact on the ion and neutral gas is very different. This is due, in part, to the fact that Joule heating is transferred to heat in the E region over larger regions and more efficiently than precipitating particle energy [e.g., Vickrey et al., 1982]. In addition, the altitude of maximum energy deposition from Joule heating is higher than particle precipitation [Brekke and Rino, 1978].

These energy sources, however, are not completely separable in their contribution to the total heating rate of the E region. For example, precipitating electrons into the ionosphere indicate the presence of an upward field-aligned current that is associated with a converging electric field. The energetics of the particle precipitation that enhance the E-region conductances and the coincident location of the enhanced conductances with the converging electric field will significantly impact the Joule heating rate. This was demonstrated, for example, by Vickrey et al. [1982] who showed that the magnitude of energy input by precipitating particles (maximizing in the morning sector) often has the opposite asymmetry about midnight to that of Joule heating (maximizing in the dusk sector). Solar EUV radiation has an important indirect contribution to the net heating of the high-latitude E region as it is a principal source of E-region ionization and conductivity. Robinson and Vondrak [1984] demonstrated that the conductance produced by solar illumination during solar minimum is comparable to that produced by the diffuse aurora and far exceeds the diffuse aurora during solar maximum conditions. The uniform distribution in conductivity caused by solar illumination and the uncoupled nature of the process to large-scale changes in the electric field can result in the solar illumination indirectly having a major contribution to the heating of the E region.

The Defense Meteorological Satellite Program (DMSP) has demonstrated that the Joule heating rate in the high-latitude ionosphere can be estimated from spacecraft [Rich et al., 1987; 1991]. These estimates of the Joule heating rate are subject to a number of assumptions that require validation. Independent ground observations of the same heating process have, therefore, been employed to test the validity of some of these assumptions. The NSF incoherent-scatter radar located at Sondrestrom, Greenland, can measure the plasma parameters of interest and is at a latitude well-suited for coincident measurements with DMSP. Until recently, the radar facility

had its limitations in accounting for the effects of the neutral wind on the Joule heating rate in the E region. However, the recent improvement in altitude resolution and signal statistics in the E region has permitted the Joule heating rate to be more accurately determined. Also, the manner in which the Joule heating rate is now being calculated parallels that of Rich et al. [1987] allowing a more direct means of testing assumptions and comparing results.

This report summarizes the progress made over the program year and details the observational program for conjunctions with the F12 and F13 DMSP satellites and the radar. Also discussed are the advancements made by the radar and the improved accuracy in determining the Joule heating rate that can now be gained by using the high-resolution radar mode. A subsequent report will detail the improvements in applying the UNTANGLE approach to the high-resolution data and describe the efforts made in validating the conductivity profile.

## **2. Program Progress**

Over the course of the program year, we have completed a number of the tasks stated in the original statement of work. The following restates the individual tasks and provides the level of accomplishment.

**Task 1:** Implement and test the radar operating model designed for DMSP coordination prior to spacecraft launch, and supply sample data to Phillips Laboratory (PL).

**Status:** Completed

Coordination with spacecraft overpasses requires the radar to make plasma measurements as a function of latitude, longitude, and time. Under the F7 program, attempts were made to obtain exact spatial and temporal coincidence with the satellite during its overpass using rapid radar elevation scans. In order to derive the full ion vector from the scan data (the key parameter for Joule heating) required certain assumptions; the conclusions from the reported results [Watermann and de la Beaujardiére, 1990] suggest that these assumptions may not always be valid. In addition, further assumptions, not considered at the time of the F7 study, were imposed to derive the conductivity and ion drift from the scan data. These assumptions concern the effects of radar pulse smearing on the derived parameters, such as electron density and ion velocity. For the F7 study, a 48 km radar pulse (long pulse) was used during the scans to provide adequate signal statistics for the determination of the electron density (used in the conductivity calculation) and ion velocity. However, pulse smearing caused by the 48 km pulse can have a significant impact on how well these parameters are determined irrespective of noise and will have important consequences when determining the Joule heating rate. An example of this effect is shown in a separate section.

Since the F7 study, the Sondrestrom radar has improved its range resolution to as good as 3 km using an alternating code pulse scheme (see Section 4). This pulse scheme reduces pulse

smearing effects significantly and, although limited by statistical noise, yields far superior measurement statistics when compared to multipulse techniques with similar range resolutions. The signal statistics are improved by operating the radar in a fixed position mode and integrating the data for a period of about 1 minute. Further range integration can be achieved in post-processing software. Therefore, rather than trying to obtain exact temporal coincidence with the satellite pass by performing fast elevation scans with a 48 km pulse and having to deal with the problems discussed above, our emphasis has been the development of an observing mode that provides a direct, and highly accurate, characterization of background plasma density and drift from a sequence of fixed-position measurements. This choice of approach is limiting in one sense: the sequence of measurements, taken over the volume of interest, requires about 25 minutes to complete. This can be reduced if the spatial resolution of the chosen volume is reduced. Inherently, then, there is the assumption that there is some degree of homogeneity and temporal stability within the ionosphere. There will be times when the dynamics of the plasma invalidates these assumptions, but with many opportunities for coincidence, data will also be collected under stable magnetic conditions. In those cases, the plasma density and ion drift can be carefully mapped at high range resolution.

**Task 2:** Establish the criteria for radar coordinated runs based upon satellite geometry and geophysical conditions, and implement procedures to schedule radar observations as frequently as site commitments allow.

**Status:** Completed

Criteria for selecting DMSP passes in conjunction with Sondrestrom radar operations are as follows:

- The E-region footprint of the DMSP pass is within 100 km of the Sondrestrom radar.
- The pass is oriented near the magnetic meridian—that is, perpendicular to the L-shell, to allow for nearly maximum latitudinal extent of the radar measurement. This refers to the ascending node of F12 and F13 orbits. These passes are typically in the dusk to midnight local time sectors, i.e., the ascending node of the orbit.
- The period of observation should be during active times. This is crudely estimated by looking at the past 3 months of daily Kp and projecting the periods of active times to the current month. The quiet times seem to be more reproducible so avoidance of those times may also better our chances of geomagnetic activity during the pass.
- The period of observation should not conflict with other radar experiments requested for the month.

These criteria typically lead to the availability of 5 to 10 orbits per month from which to choose for coordinated observations with the radar. About 12 to 15 hours per month of radar time are dedicated to DMSP experiments. Each experiment is of 3-hour duration centered on the time of the pass resulting in about 4 to 5 passes chosen each month.

**Task 5:** Establish a format for summarizing radar data, and supply those data on a timely basis to PL throughout the period of observations.

**Status:** Completed

We have compiled summary plots of the data that will constitute a catalogue of observations for a quick overview of the radar data taken during DMSP passes. This involves analyzing the long-pulse data from elevation scans and dwells to give us an indication of the ionospheric conditions during the DMSP flyby. If the conditions are favorable (i.e., if significant structure is present in the E region), we can then begin to analyze the complete radar data set. The catalogue is in hard copy form and can be accessed through SRI.

**Task 3:** In conjunction with PL, select optimum algorithms and atmospheric models for use with the satellite and radar computation of Joule heating rate, and adapt the radar software to use those algorithms and the A16B high-resolution radar data.

**Status:** In Progress

The development of the Joule heating rate calculations from the radar using the new high-resolution radar mode is described in Section 5. Based on these calculations a number of important assumptions used in previous radar calculations and in the DMSP calculations can be investigated. We are currently in the process of assessing the impact of those assumptions.

**Task 4:** Evaluate the photoionization model used by PL using data recently collected at Sondrestrom, including consideration of data confidence intervals, and suggest a short-term photoionization dependence if deemed necessary.

**Status:** In Progress

When the ionosphere is fully sunlit, photoionization dominates the Pedersen conductivity, and is thus an important factor for the global Joule heating measurements. One of the conclusions of the previous DMSP/radar study was that the model for estimating the solar photoionization [Robinson and Vondrak, 1984] may be in error or is not applicable at Sondrestrom. This model can now be tested from a number of summer data sets taken over the course of 3 years using the high-resolution mode.

The high-resolution radar data also make it possible to evaluate the validity of assumptions that are made about the E-region conductivity calculations based on the measured particle flux. The ionospheric conductivity is estimated by assuming that the precipitating particles have certain characteristics [Robinson et al., 1987]. In particular, it assumes that the only flux is of downward electrons, the energy distribution is Maxwellian, and the particles are limited to an energy range between 500 eV and 30 keV. Within these constraints, and under the assumption that the neutral atmosphere model is accurate, the conductivity and electron density can be estimated and can be compared to the radar-observed distributions. Robinson et al. [1987] have found that the particle distribution simplifications are appropriate, but the overall accuracy of the

conductance depends upon the proper choice of the energy limits between which the particle characteristics are computed and the proper velocity distribution of the precipitating particles.

**Task 6:** Perform detailed analysis of selected satellite/radar data sets in order to determine the sensitivity of the Joule heating estimates to a neutral model and other assumptions.

**Status:** To be developed

**Task 7:** Maintain a statistical database of radar-observed Joule heating observations collected over the duration of the project.

**Status:** To be developed

### 3. ISR Observing Periods and Geomagnetic Conditions

Twenty-seven radar experiments dedicated to DMSP overpasses have been carried out over the program year. These experiments used the transmitter mode and the specialized antenna mode designed for DMSP volume studies described in previous reports. Table 1 provides some of the details for each of the experiments. It should be noted that other radar operations, not included in Table 1 but coincident with DMSP flybys, which could benefit the DMSP study, may have occurred during this period. The experiments in Table 1 consist of a combination of orbits that passed near the magnetic meridian (dusk passes) and orbits that were more aligned in the magnetic east-west direction (prenoon passes). A hardware problem arose in the high-resolution A16 mode that contaminated the autocorrelation functions preventing us from determining the necessary high-resolution ion drift velocity, ion and electron temperature, and corrected electron density information from data taken between 26 September 1995 and 29 November 1995. The long pulse data and the high-resolution density not corrected for temperature recorded during this period were not affected by this problem and, so, some limited information on the Joule heating rate and conductivity can be determined, if this period is of significant interest. Table 2 lists the solar flux and geomagnetic activity indices of 3-hour  $K_p$  and the daily  $A_p$ . The UT corresponding to the stop time of the experiment was used to determine the current  $K_p$  value with the prior 6 hours of  $K_p$  included to cover conditions before and during the experiment.

Based on geomagnetic indices during the experiments and the structure of the ionosphere from the elevation scans and dwells, we have identified a number of experiments that may be suitable for high-resolution analysis of the Joule heating rate. The dates for these experiments are 21 June, 1 July, 16 July, 30 July, and 7 August 1995. A sample of quick-look data plots for the 21 June data set is shown in the Appendix. Plots of the electron density for that experiment are preceded by a polar plot of the radar azimuth and elevation positions during the experiment and the track of the DMSP satellite projected along magnetic flux tubes to an altitude of 125 km. The arrangement of electron density plots is in chronological order, with the first plot being an

**Table 1. Sondrestrom Radar Operations for Primary DMSP Passes**

<u>Day No.</u>	<u>Date</u>	<u>Start UT</u>	<u>Stop UT</u>	<u>Satellite</u>	<u>Azimuth</u>	<u>Antenna File</u>	<u>Remarks</u>
076	950317	2130	2359	f12	n-s	f12p002	comp scan
081	950322	1336	1446	f12	e-w	f12p003	comp scan
089	950330	1319	1430	f12	23	f12p004	
152	950601	0932	1053	f13	32	f1395152	active
155	950604	1910	2012	f13	157	f1395155	
160	950609	2233	2351	f12	158	f1295160	
172	950621	1859	2001	f13	151	f1395172	(world day)
177	950626	0944	1045	f13	28	f1395177	
177	950626	2217	2332	f12	154	f1295177	
182	950701	1308	1430	f12	22	f1295182	
185	950704	0952	1053	f13	23	f1395185	
197	950716	1854	2008	f13	155	f1395197	active
199	950718	1312	1441	f12	21	f1295199	
202	950721	0947	1048	f13	22	f1395202	active
207	950726	1334	1438	f12	23	f1295207	
211	950730	2241	2347	f12	154	f1295211	active
214	950802	1850	2006	f13	154	f1395214	structured
219	950807	2221	2323	f12	155	f1295219	E <sub>s</sub>
236	950824	2250	2333	f12	154	f1295236	too windy
239	950827	1902	2009	f13	155	f1395239	quiet
241	950829	1332	1434	f12	22	f1295241	
244	950901	0948	1050	f13	22	f1395244	
252	950910	2237	2350	f12	154	f1295253	
256	950913	1903	2004	f13	154	f1395256	active
269	950926	0925	1023	f13	22	f1395269	A16 problem
295	951022	2217	2352	f12	n-s	f1295295	A16 problem
303	951030	0752	1100	f13	e-w	DMSPns	A16 problem

**Table 2. Geomagnetic Conditions During DMSP Passes**

<u>Date</u>	<u>UT</u>	<u>F10.7</u> <u>(prior day)</u>	<u>F10.7</u> <u>(81-day average)</u>	<u>K<sub>p</sub></u> <u>(UT-0 hr)</u>	<u>K<sub>p</sub></u> <u>(UT-3 hr)</u>	<u>K<sub>p</sub></u> <u>(UT-6 hr)</u>	<u>A<sub>p</sub></u> <u>(daily)</u>
950317	2359	83.3	82.6	2.0	2.3	2.7	8.0
950322	1446	89.3	81.8	0.7	0.7	1.0	3.0
950330	1430	80.7	81.1	3.0	1.7	1.3	8.0
950601	1053	70.9	77.6	3.3	3.7	4.0	25.0
950604	2012	76.8	77.6	2.0	2.3	1.7	6.0
950609	2351	86.8	77.9	1.7	1.7	1.7	5.0
950621	2001	74.2	77.4	2.0	2.3	2.3	10.0
950626	1045	73.2	76.8	2.7	3.3	4.0	17.0
950626	2332	73.2	76.8	3.0	3.0	2.3	17.0
950701	1430	80.8	76.1	1.7	2.0	2.7	13.0
950704	1053	80.7	76.2	0.7	1.3	2.3	7.0
950716	2008	76.8	76.4	4.3	6.0	5.3	30.0
950718	1441	74.7	76.3	3.3	2.3	2.0	10.0
950721	1048	72.0	76.0	1.7	1.3	0.7	5.0
950726	1438	72.0	75.7	1.7	1.0	1.3	5.0
950730	2347	72.0	75.7	3.0	1.7	1.7	6.0
950802	2006	74.8	75.5	2.7	2.0	1.3	5.0
950807	2323	77.3	75.3	3.0	3.0	2.0	8.0
950824	2333	75.9	73.8	2.3	2.0	1.7	6.0
950827	2009	78.9	73.6	2.3	1.7	1.3	7.0
950829	1434	83.2	73.6	2.0	3.3	2.3	10.0
950901	1050	77.0	74.0	0.7	0.3	0.7	4.0
950910	2350	69.7	75.4	4.7	3.3	2.3	12.0
950913	2004	69.5	75.5	2.3	3.0	2.7	18.0
950926	1023	74.5	75.3	2.0	1.3	1.7	4.0
951022	2352	80.3	74.5	2.7	3.7	1.7	12.0
951030	1100	72.8	74.6	1.7	0.3	0.0	12.0

elevation scan followed by the sequence of dwells plotted in altitude versus time and completed with a final elevation scan. The contour plots of the log of the electron density are in units of  $\times 10^{11} \text{ m}^{-3}$  at an interval of 0.5.

A summary of the conditions during each experiment follows, in order of best-to-least contribution to the study:

- Experiment 950621  
Active conditions with E-region arc to the north of the site exceeding  $3.0 \times 10^{11} \text{ m}^{-3}$  persisting throughout the experiment.
- Experiment 950730  
Relatively quiet until about 23:40 UT when an E-region arc with densities in excess of  $5 \times 10^{11} \text{ m}^{-3}$  is apparent in the last few dwells to the south and in the subsequent elevation scan.
- Experiment 950716  
Active conditions with some E-region structure to the south near 19:30 UT during the dwell sequence.
- Experiment 950701  
Uniform E region throughout the experiment. Little indication of E-region structure; however, good signal statistics for high-resolution mode with E-region densities above  $1.0 \times 10^{11} \text{ m}^{-3}$ .
- Experiment 950807  
No apparent activity throughout the experiment with a uniform E region of densities below  $1.0 \times 10^{11} \text{ m}^{-3}$ .

#### 4. Radar Technique

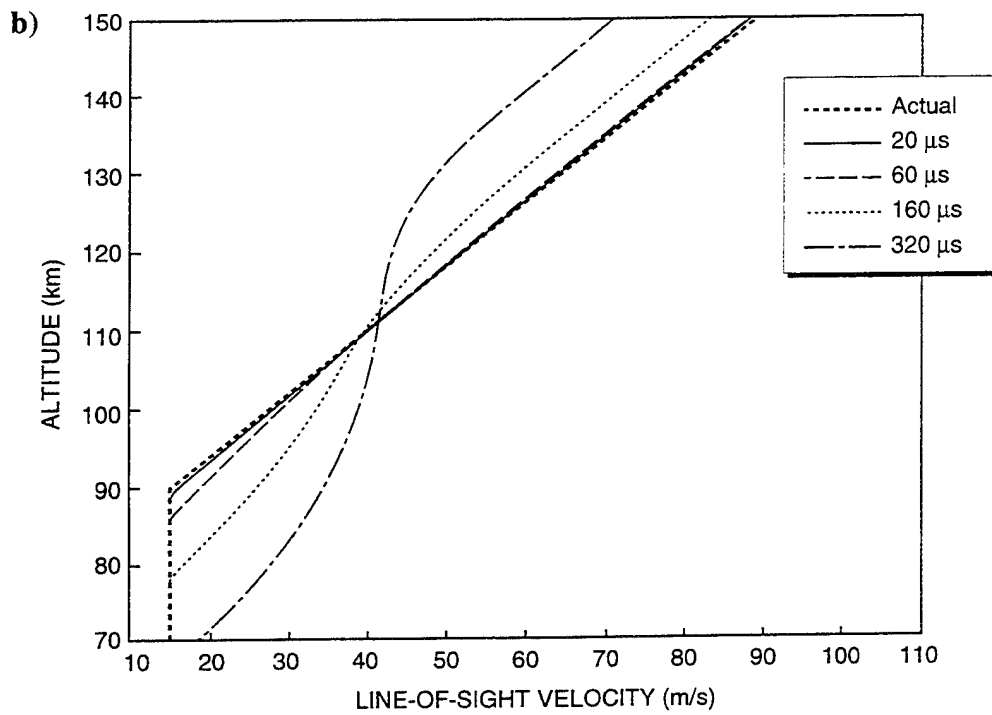
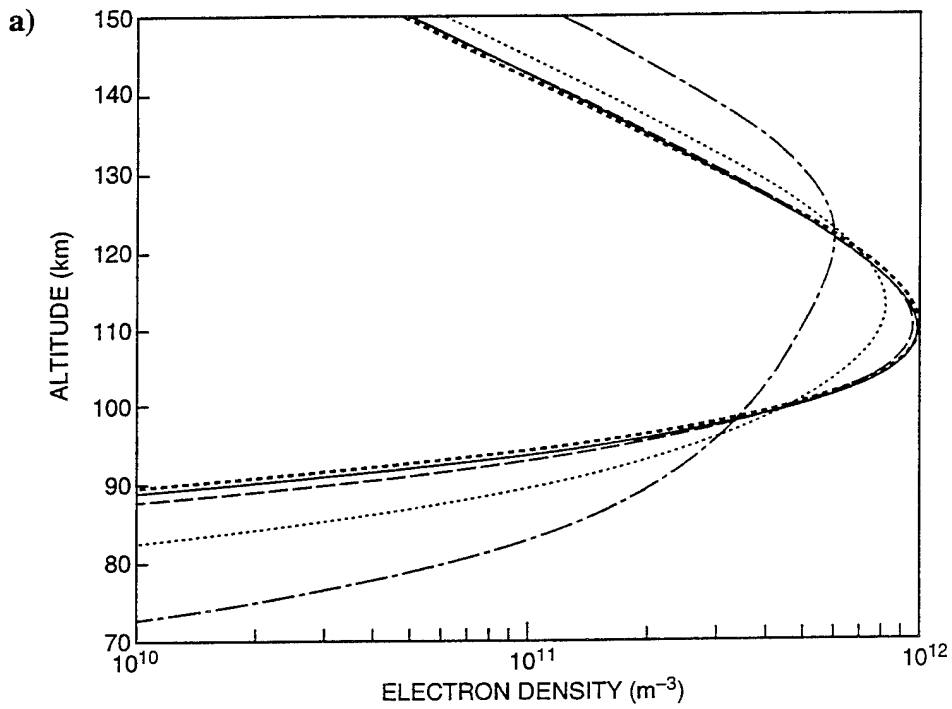
Incoherent-scatter radar measurements provide the most comprehensive measurement set for estimating the local current, electric field, and conductivity throughout the E region. Neutral winds are also derivable from the radar measurements but are generally limited to altitudes below about 125 km due to the increasing sensitivity to uncertainties in the collision frequency with height along with a dependency on the orientation of the E field. The explicit calculation of the neutral winds in the E region is not necessary if the Joule heating rate is determined by measuring the current density in the E region, as discussed in the next section. The radar measurements needed to determine the E-region currents are E-region electron density profiles, E-region ion velocity profiles, and F-region ion velocities.

Considerable progress has been made over the years toward improving the measurement of these quantities with the Chatanika/Sondrestrom radar. Prior to late 1973, the system capabilities consisted of velocity measurements with no better than 48 km range resolution (from a long 320  $\mu$ s pulse), electron density profiles from that same pulse, and power profile measurements from a 9 km or 60  $\mu$ s pulse. For an incoherent-scatter radar, the received power profiles can be converted to electron density profiles if additional information about the electron-to-ion temperature ratio is also available. Temperature information to correct the 9 km pulse for electron density were taken from the long pulse measurements. Thus, with a number of assumptions (some of which may have affected the results significantly) it was possible to estimate E-region electron density profiles with 9 km resolution, an average E-region ion velocity, and an F-region velocity.

Modifications were made to the radar system in 1973 to provide a multipulse capability. This permitted, among other things, the measurement of temperatures and velocities through the E region with approximately 9 km range resolution. Unfortunately, the signal statistics were rather poor for the 9 km multipulse scheme and it was primarily useful only during auroral events. Using the same multipulse hardware, a compromise single pulse algorithm was implemented that used a 160  $\mu$ s pulse yielding 24 km range resolution. The signal statistics for this were far superior to the 9 km multipulse.

Figure 1 illustrates the impact of these various pulse widths on the measurements that can be made by a radar. A simple Chapman layer was assumed for the actual electron density in that figure and the effect of the pulse smearing was simulated (including r-squared effects). The figure shows the dramatic change in the radar-measured density profiles in the E region for both 320 and 160  $\mu$ s pulses. The peak electron densities are greatly misrepresented (note the log scale) and, even more significantly, the bottom side of the E region is lowered by over 10 km for the 320  $\mu$ s pulse. The second panel in Figure 1 shows that the velocity measurements are also significantly affected—especially by the 320  $\mu$ s pulse. The move to a multipulse scheme (60  $\mu$ s or 160  $\mu$ s) very effectively reduced the magnitude of the velocity errors and the range smearing effects on the density. Unfortunately, as mentioned above, the 60  $\mu$ s multipulse also resulted in significantly degraded signal statistics. It should be noted that above about 200 km the pulse-smearing effects for both the 160 and 320  $\mu$ s pulses are negligible due to a more extensive and slowly varying F region with height.

In the late 1980's, the on-line data processing hardware at Sondrestrom was replaced with more readily available off-the-shelf hardware that provided greater flexibility in implementing sophisticated operating modes. As a result, new high-resolution operating modes, such as multipulse algorithms [Farley, 1972] and an alternating code algorithm [Lehtinen, 1986; Lehtinen and Haggstrom, 1987], were implemented at Sondrestrom. The alternating code technique [Lehtinen, 1986; Lehtinen and Haggstrom, 1987] yields far superior measurement statistics when compared to multipulse techniques with similar range resolutions and became our standard high-resolution mode in 1993. The Sondrestrom implementation of alternating codes



6536ar1/f1

Figure 1 Effects of pulse smearing on the a) electron density and b) line-of-sight velocity in the E-region for transmitted radar pulses of 20  $\mu\text{s}$  (3 km), 60  $\mu\text{s}$  (9 km), 160  $\mu\text{s}$  (24 km), and 320  $\mu\text{s}$  (48 km) widths.

(called A16 for 16 baud alternating code) uses 20  $\mu$ s bauds that result in 3.0 km range resolutions, which has little impact on the electron density and ion velocity shown in Figure 1. This development is based on the implementation of transmitter modes using the alternating code technique. It is a close relative of the coded long pulse technique [Sulzer, 1986] in that the high range resolution is obtained via cancellation of the contributions of lag products from unwanted ranges. This is in contrast to other pulse compression techniques, like Barker codes or complementary codes, which rely on cancellation at the voltage level and, as a result, require that the correlation time of the media be longer than the entire code sequence. In fact, Lehtinen [1986] and Lehtinen and Haggstrom [1987] point out that additional range resolution can be obtained by combining the techniques; phase coding the individual bauds of the alternating codes.

The standard transmitter mode now used most often, and exclusively in this DMSP study, is the SA16C mode. The SA16C mode consists of standard uncoded 320  $\mu$ s long pulse at one frequency (S) and 32 separate pulses, each with different phase code, on the other frequency (A16C). The alternating code yield lags 1 through 15 with a baud length/lag spacing of 20  $\mu$ s. To obtain the zero lag of the autocorrelation function (ACF) a simple 20  $\mu$ s pulse is transmitted with each of the 32 pulses making up the alternating code scheme. The end result is a set of ACFs from the long pulse mode at 48 km range resolution and a set of ACFs from the alternating code mode at 3 km range resolution. The long pulse data can be used for estimates of plasma parameters in the F region while the alternating code data are used for estimates of plasma parameters in the E region.

Once the ACFs are recorded, for a given on-line integration, the data are processed where improvements in signal statistics can be made through further range and time integration. The processed ACFs are then analyzed using a nonlinear least squares approach to determine the corrected electron density, electron temperature, ion temperature, ion velocity, collision frequency, and composition. The technique used to fit the measured ACF involves the computation of a theoretical ACF and an unconstrained optimization procedure to perform numerical minimization based on the Levenberg-Marquardt method for each recorded range gate [Zambre, SRI Internal Report, 1993]. The error bars associated with each of the fitted parameters correspond to confidence intervals at the one-sigma level of 68.26%. In the data used for the analysis of the Joule heating rate and the conductivity the primary fitted parameters used will be the corrected electron density and the ion velocity.

The radar approach described above differs in many ways from the F7/radar study of the Joule heating rate by Watermann and de la Beaujardi re [1990]. First, we employ short pulse widths of 3 km that do not significantly smear the return signal and improves dramatically the retrieval of electron density and ion velocity from the measurement. This improved measurement allows for improved accuracy in conductivity and a new and accurate estimate of the E-region current density within the E region. Because of the new current density measurements, estimates of the Joule heating rate can be made more accurately, including neutral wind effects. The approach also parallels that used in the DMSP analysis providing a more

direct comparison between techniques. The only limitation to the new approach is the need to perform minute integrations per position to achieve the necessary signal statistics. This results in a temporal resolution limit of a few minutes, which, we feel, is warranted given the improvements. In addition, data are recorded in a similar fashion as the F7/radar study so that comparisons can be made to verify the assumptions made in the previous study.

## 5. ISR Estimates of the Joule Heating Rate

Much work has been done on quantifying the dissipation rate of electromagnetic energy in the ionosphere through calculations of the Joule heating rate. The scientific impetus for determining the Joule heating rate in the ionosphere can be separated into two general categories: 1) to determine the “dissipative load” on the magnetosphere so that the magnetospheric energy flux required by the ionosphere–thermosphere system can be quantified, and 2) to determine the effects of Joule heating on the ionosphere–thermosphere system. Many of these investigations have used the expression

$$q_j = j_{\perp} \cdot E' = \sigma_p E'^2 = \sigma_p (E + u_n \times B)^2 \quad (1)$$

and have required the need to make some approximations to the Joule heating calculation. This is due to the fact that to accurately evaluate the Joule heating rate by (1), height integrated or not, requires knowledge of the electric field and the height distribution of the neutral wind and conductivity (requiring collision frequency and gyrofrequency calculations based on plasma and neutral composition). This was the approach used in the previous radar/DMSP Joule heating study as described by Watermann and de la Beaujardi re [1990]. In that study it was generally assumed that the neutral wind was negligible and that a 48 km radar pulse was sufficient in describing the E-region electron density and, consequently, the height-integrated conductivity. As was shown in the previous section, the long pulse mode is not appropriate for estimating the E-region electron density when the E region is significantly structured.

Another approach to estimating the Joule heating rate that was discussed by Cole [1975] but that is not, in general, used is the expression

$$q_j = j_{\perp} \cdot E'_{\perp} = \frac{j_{\perp}^2}{\sigma_c} \quad , \quad (2)$$

where  $\sigma_c$  is the Cowling conductivity given by

$$\sigma_c = \sigma_p + \frac{\sigma_H^2}{\sigma_p} \quad , \quad (3)$$

with  $\sigma_p$  and  $\sigma_H$  the symbols for the local Pedersen and Hall conductivity, respectively. Because this expression involves the difficult measurement of the local current density and the Cowling conductivity in the E region, many investigations have not used this approach. However, using

(2) has the advantage that the effects of the neutral wind on the Joule heating rate are inherently contained within the current density measurement and the only significant model parameter needed in (2) is the collision frequency.

Incoherent-scatter radar observations have been particularly successful in estimating the Joule heating rate in the ionosphere at high spatial and temporal resolution. Both approaches given by (1) and (2) have been used in estimating the Joule heating rate from incoherent-scatter radar measurements. The first and more typical approach involves determining the electric field and Pedersen conductivity throughout the E and F regions and either including local effects by the neutral wind [de la Beaujardiére et al., 1991] or setting the neutral wind to zero. This approach is generally associated with radar measurements that are not able to determine accurately the currents in the E region. However, Brekke and Rino [1978] determined E-region currents from incoherent-scatter radar measurements at Chatanika using a pulse scheme that provided sufficient (~10 km) resolution, albeit with significantly limited SNR, and evaluated empirically the Joule heating rate using the expression given by (2). As discussed by Brekke and Rino [1978], the height of maximum Joule heating rate estimated by (1) is much more sensitive to the model collision frequency (and, therefore, the model neutral atmosphere) than that estimated by (2). Given the new high-resolution mode implemented at the Sondrestrom radar, (2) may be used in the evaluation of the E-region Joule heating rate with much better accuracy than the previous DMSP study. *An important comparison that may be done with the radar is to test assumptions that have been employed using (1) with the more accurate determination of the Joule heating rate using (2). In particular, the assumption of a zero neutral wind when using (1), as was done in the F7 DMSP/radar study, can be tested. To test this assumption, we do not require simultaneous DMSP measurements.*

Satellite measurements have also used various forms of (1) and (2) to estimate the global distribution of the height-integrated Joule heating rate [i.e., Foster et al., 1983; Rich et al., 1987; Heelis and Coley, 1988]. These measurements generally ignore neutral wind effects and model the height-integrated ionospheric conductivity. Foster et al. [1983] examined the seasonal variations in the conductivity and the square of the electric field to estimate seasonal variations in the Joule heating rate. Their results found the Joule heating rate to be 50% greater during the summer than winter because of the increased conductivity due to solar illumination. Heelis and Coley [1988] examined the relationship between the height-integrated Joule heating rate, the local F-region Joule heating rate, and the F-region ion temperatures. This study illustrated the point that knowledge of the F-region differential velocity between ions and neutrals, although useful in assessing the local behavior of the ion temperature, does not by itself infer knowledge of the local or height-integrated Joule heating rate and vice versa. Rich et al. [1987] take the interesting approach of evaluating the height-integrated Joule heating rate using (2) by assuming the ionosphere between 90 and 200 km to be a flat plate. In this case, the neutral wind is implicitly included in the height-integrated current estimate but the height-dependent relationship between the current and conductivity is ignored.

*Because the new approach used to calculate the Joule heating rate by the radar is similar to that performed with the DMSP measurements, direct validation of the flat plate assumption can be made. This is one of the key areas we will be investigating with the radar measurement that does not necessarily require coincident measurements with DMSP.*

To apply the expressions described above to incoherent-scatter radar measurements, it is best to reduce the equations in terms of the most basic parameters derived directly from the radar. This simplifies the error propagation and, although, some equations may not be intuitive they illustrate directly the variables that are measured versus those that are modeled or estimated. For example, the local current density may be written as

$$j = en_e(v_i - v_e) \quad (4)$$

with the electron density,  $n_e$ , the E-region ion drift velocity,  $v_i$ , and the electron drift velocity,  $v_e$  (assumed equal to the F-region ion drift), all directly derivable from the measurement. Using propagation of errors and ignoring correlation errors, the relative error for the current density is given by

$$\frac{\sigma_j}{j} = \sqrt{\frac{\sigma_{n_e}^2}{n_e^2} + \frac{\sigma_{v_i}^2}{\Delta v^2} + \frac{\sigma_{v_e}^2}{\Delta v^2}} \quad (5)$$

with  $\sigma$  representing the one-sigma error and  $\Delta v$  representing the drift velocity difference between the E region and F region drifts for a particular E region altitude. Thus, the error in the current calculation grows as the differential velocity between the E and F region drifts gets small for a given accuracy in the drift measurement. This limits the ability to determine currents accurately above the E region using this approach.

For the Joule heating rate, (2) becomes

$$j \cdot E' = q_j = \frac{j^2 B \omega_i}{en_e v_{in}} \quad (6)$$

illustrating its dependence on the inverse of the modeled ion-neutral collision frequency. The relative error for the Joule heating rate is given as

$$\frac{\sigma_{q_j}}{q_j} = \sqrt{\frac{\sigma_{n_e}^2}{n_e^2} + \frac{\sigma_{v_{in}}^2}{v_{in}^2} + \frac{4\sigma_j^2}{j^2}} \quad (7)$$

Here, the error in the Joule heating rate is most sensitive to errors in the current density and, therefore, calculations of the Joule heating rate using this approach is also limited to E-region altitudes (< 140 km).

## 6. References

- Banks, P. M., "Observations of Joule and Particle Heating in the Auroral Zone," *Journal of Atmospheric and Terrestrial Physics*, Vol. 39, pp. 179-193, 1977.
- Brekke, A., and C. L. Rino, High-resolution altitude profiles of the auroral zone energy dissipation due to ionospheric currents, *J. Geophys. Res.*, 83, A6, 2517-2524, 1978
- Cole, K. D., "Energy Deposition in the Thermosphere Caused by the Solar Wind," *Journal of Atmospheric and Terrestrial Physics*, Vol. 37, pp. 939-949, 1975.
- de la Beaujardiére, O., R. Johnson, and V. B. Wickwar, "Ground-Based Measurements of Joule Heating Rates," *Auroral Physics*, pp. 439-448, 1991.
- Farley, D. T., Multiple-Pulse Incoherent-Scatter Correlation Function Measurements, *Radio Science*, 7, 661-666, 1972.
- Foster, J. C., J. -P. St. -Maurice, and V. J. Abreu, "Joule Heating at High Latitudes," *Journal of Geophysical Research*, Vol. 88, No. A6, Pages 4885-4896, 1983.
- Heelis, R. A., and W. R. Coley, "Global and Local Joule Heating Effects Seen by DE 2," *Journal of Geophysical Research*, Vol. 93, No. A7, pp. 7551-7557, 1988.
- Lehtinen, M. S., Statistical Theory of Incoherent Scatter Measurements, Ph.D. thesis, Univ. of Helsinki, Helsinki, 1986 (EISCAT Technical Note 86/45).
- Lehtinen, M. S., and I. Haggstrom, "A New Modulation Principle for Incoherent Scatter Measurements," *Radio Sci.*, 22, 4, 625-634, 1987.
- Rich, F. J., M. S. Gussenhoven, and M. E. Greenspan, "Using Simultaneous Particle and Field Observations on a Low Altitude Satellite to Estimate Joule Heat Energy Flow Into the High Latitude Ionosphere," *Annales Geophysicae*, pp. 527-534, 1987.
- Rich, F. J., M. S. Gussenhoven, D. A. Hardy, and E. Holeman, "Average Height-Integrated Joule Heating Rates and Magnetic Deflection Vectors Due to Field-Aligned Currents During Sunspot Minimum," *Journal of Atmospheric and Terrestrial Physics*, Vol. 53, No. 3/4, pp. 293-308, 1991.
- Robinson, R. M., and R. R. Vondrak, "Measurements of E Region Ionization and Conductivity Produced by Solar Illumination at High Latitudes," *Journal of Geophysical Research*, Vol. 89, No. A6, pp. 3951-3956, 1984.
- Robinson, R. M., R. R. Vondrak, K. Miller, T. Dabbs, and D. Hardy, "On Calculating Ionospheric Conductances From the Flux and Energy of Precipitating Electrons," *Journal of Geophysical Research*, Vol. 92, No. A3, pp. 2565-2569, 1987.

- Sulzer, M. P., "A Radar Technique for High Range Resolution Incoherent Scatter Autocorrelation Function Measurements Utilizing the Full Power of Klystron Radars," *Radio Sci.*, 21, 6, 1033-1040, 1986.
- Vickrey, J. F., R. R. Vondrak, and S. J. Matthews, "Energy Deposition by Precipitating Particles and Joule Dissipation in the Auroral Ionosphere," *Journal of Geophysical Research*, Vol. 87, No. A7, pp. 5184-5196, 1982.
- Watermann, J., and O. de la Beaujardiére, "Joule Heating Investigations Using the Sondrestrom Radar and DMSP Satellites," Final Report, June 1990.

**Appendix**

**Sample of Quick-Look Data Plots for 21 June Data Set**



TOPIC --- ELEVATION (M) PLOTTER ON 01113

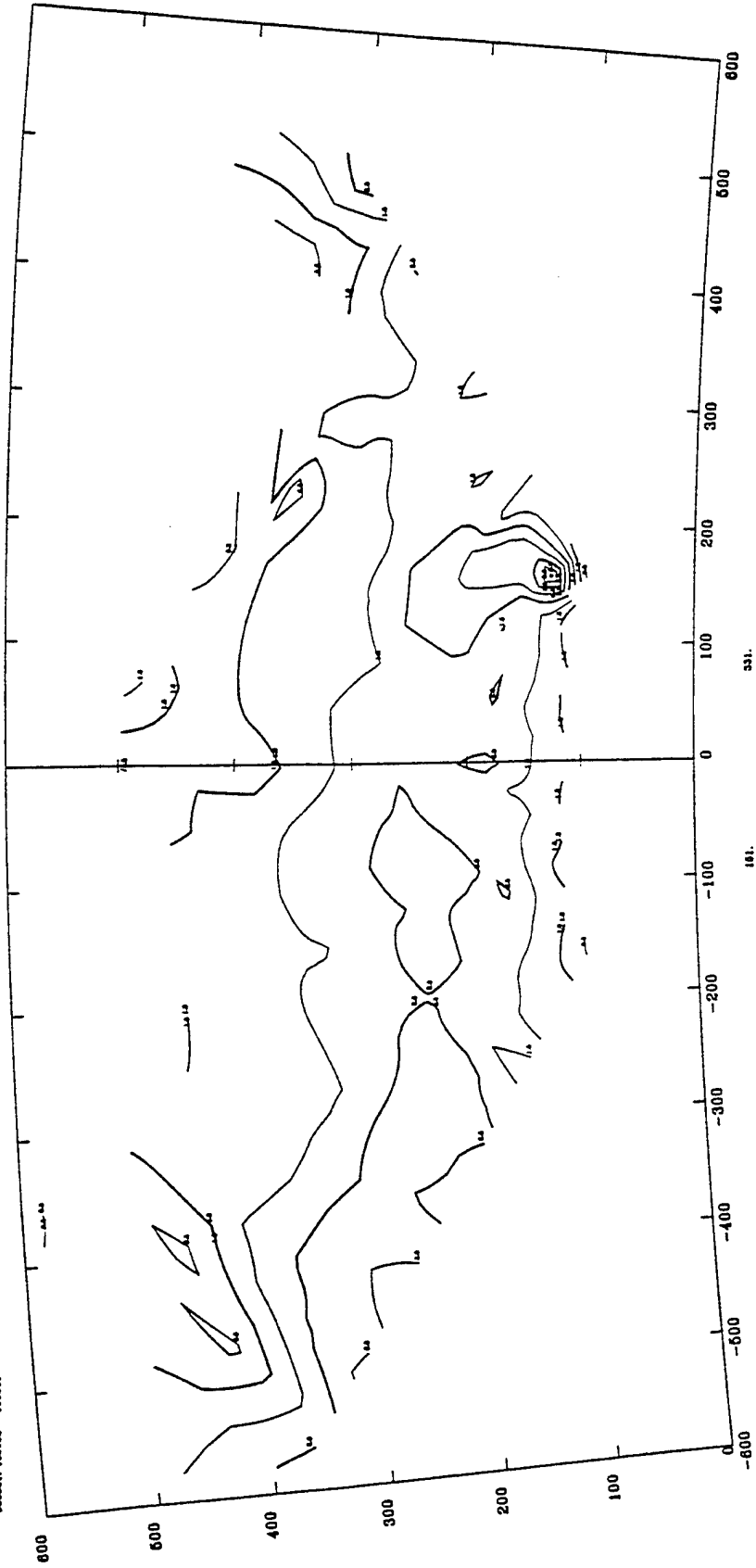
630 - LOGIC (M IN M-3)

UNITA LOG(M-3) 2100-11

ALLOWED ERROR ----- TOLERANCE 0.07% ALLOWED GAP: 0.0 SECURES

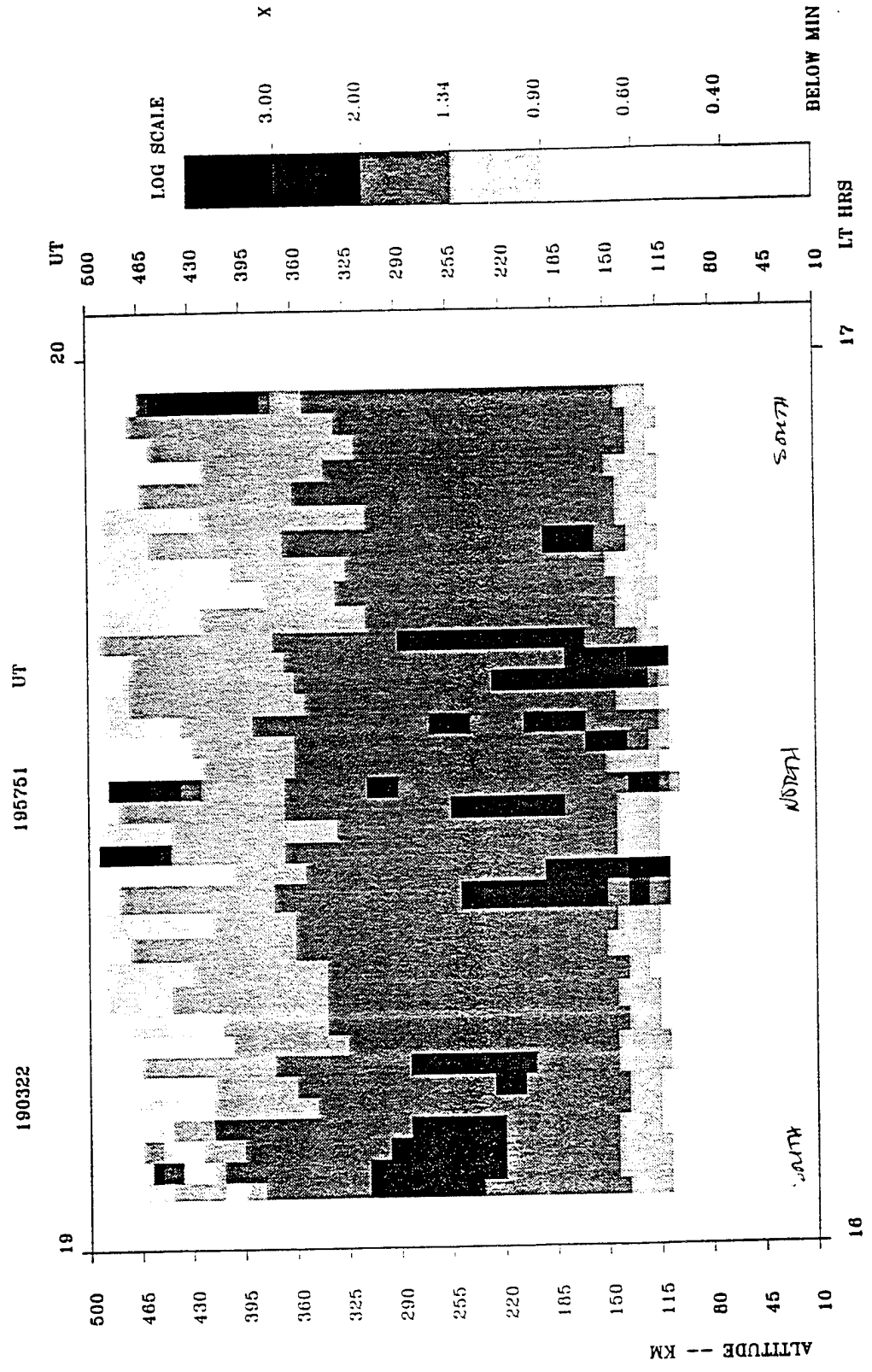
PULSE = 210 10 MS/INT

60001: 151045 - 100027



SONDRESTRÖM

950621 TO 950621



NE (EL/M\*\*3) LONGPULSE

TABLE -- ELEVATION DATA PLOTTED ON 81113

820 - 10018 (NE IN N-3)

UNIT: 10018-3 0100-11

ALLOTTED ERROR: ----- TOLERANCE: 0002 ALLOTTED GAP: 80 DEGREE

PULSE = 320 10 000 INT

8000011 100000 - 800100

